Structure of Instantaneous Reynolds Stress over a Permeable Open-channel with Suction or Injection

By

Hiroji NAKAGAWA* and Iehisa NEZU*

(Received February 14, 1979)

Abstract

In the present study, we investigate experimentally the structure of the instantaneous Reynolds stress in open-channel flow over a permeable bed with suction or injection.

Then, the fluctuating signals obtained from the X-type hot-films are conditionally analyzed in order to examine the effect of suction or injection on the turbulence production mechanism or the bursting phenomenon. We can then obtain the following results. The absolute magnitudes of the turbulence intensities and the Reynolds stress near the wall increase with an enlargement of the injection, while they decrease with an enlargement of the suction. However, the fraction of time occupied by each bursting event and the contributions of its event to the Reynolds stress against any hole size are almost the same, irrespective of suction or injection. The promotion of turbulence by injection or its suppression by suction may be caused by similar variations of three parameters of the bursting intensity, the bursting period and the bursting duration time. To sum up, the internal structure of the turbulence or the bursting mechanism is not essentially influenced by suction or injection, as long as the flow is still turbulent.

1. Introduction

In the last decade intensive experimental research on the turbulence-production mechanism and the bursting phenomenon over a smooth *solid* bed has been performed by making use of various visual methods and conditional point-measurements such as hot-wire or hot-film anemometers. As the result of this research, the physics of solid-wall turbulence have now been established in at least a qualitative sense. For example, Hinze(1975)[1] and Willmarth(1975)[2] have written excellent reviews which describe the recent status of research on solid-wall turbulence, especially on the bursting phenomenon over turbulent boundary layers. Also, they have pointed out the necessity of

*) Department of Civil Engineering

research on the structure of instantaneous Reynolds stress in order to make clear the bursting phenomenon near the wall. The authors(1977)[3] have investigated in detail the contributions to the Reynolds stress from bursting events in open-channel flows by conditionally analyzing the instantaneous Reynolds stress fluctuations obtained from the hot-film anemometers. Furthermore, on the basis of the knowledge obtained from these investigations, the authors(1978)[4] have recently proposed a simple mathematical simulation model of the bursting process, i. e. a renewal model, and have obtained a quantitative description of the bursting phenomenon over the solid open-channel.

Although the above-mentioned investigations deal with the turbulence over a *solid* bed, the turbulence characteristics over a *permeable* bed with suction or injection have been recently studied by Andersen et al. (1975)[5] and Nezu(1977)[6]. From these investigations, it has been inferred that when injection was given through the permeable bed, the turbulence above the bed became more active and in an extreme case it showed separation of the flow. However, when suction was given, the turbulence became more inactive and in an extreme case it could not keep the turbulent state any longer, and showed relaminarization characteristics. In other words, the turbulent structure may be remarkably influenced by suction or injection. Consequently, it is rightly suggested that the turbulence over a permeable bed can be reasonably controlled by giving such a transpiration, which suggestion is very important in hydraulic engineering and environmental sciences.

Therefore, in order to examine the effect of suction or injection on the turbulence production mechanism in open-channel flow, the present paper investigates the structure of instantaneous Reynolds stress over a permeable bed with suction or injection by conditionally analysing its fluctuating signals.

2. Brief recapitulation of the mean velocity distribution with transpiration[6]

Fig. 1 shows the illustration of a fully developed, two-dimensional open channel flow over a permeable smooth bed. When the transpiration velocity v_0 is given uniformly through the porous bed, the total shear stress distribution $\tau(y)$ is obtained from the equation of motion, as follows:

$$\tau/\rho = U_*^2(1-\xi) + v_0(U-\xi U_{max}) + \{\Psi(y) - \xi\Psi(h)\} \tag{1}$$

$$\Psi(y) \equiv \frac{d}{dx}\int_0^y U^2 dy - U\frac{d}{dx}\int_0^y U dy \tag{2}$$

where, $\xi \equiv y/h$, U_* is the friction velocity and U_{max} is the velocity at the free surface, i. e. $y=h$.

In order to evaluate the advection term $\Psi(y)$, we assume that there may exist a similarity of the mean velocity, i. e. $U/U_{max}=\eta(\xi)$. Hence, considering the experimental

fact that the gradient of the shear stress at the free surface isn't affected by the moderate rate of transpiration, we can obtain

$$\left.\frac{d\tau}{d\xi}\right|_{\xi=1}=\left.\frac{d\tau(v_0=0)}{d\xi}\right|_{\xi=1}\equiv -U_{*0}^2 \tag{3}$$

where, U_{*0} is the friction velocity when $v_0=0$.

From the above assumptions, (1) can be written as

$$\tau^+=(1-\xi)+v_0^+(U^+-\xi U_{max}^+)+\{\Psi^+(\xi)-\xi\Psi^+(1)\} \tag{4}$$

$$\Psi^+(\xi)\equiv\Psi(\xi)/U_*^2$$

$$=\frac{1}{\{1-\theta_2(1)\}}\left\{\left(1-\frac{1}{\Omega}\right)+\frac{v_0^+U_{max}^+}{\theta_1(1)}\right\}\theta_2(\xi)-\frac{v_0^+U_{max}^+}{\theta_1(1)}\eta\theta_1(\xi) \tag{5}$$

$$\left.\begin{aligned}\theta_1(\xi)&=\int_0^\xi\eta d\xi\\ \theta_2(\xi)&=\int_0^\xi\eta^2 d\xi\end{aligned}\right\} \tag{6}$$

where, $\Omega\equiv(U_*/U_{*0})^2$ and the (+)-suffix denote the dimensionless quantity by U_* and the kinematic viscosity ν.

The distribution of the Reynolds stress $-\overline{uv}$ is given by

$$-\overline{uv}/U_*^2=\tau^+-(dU^+/dy^+) \tag{7}$$

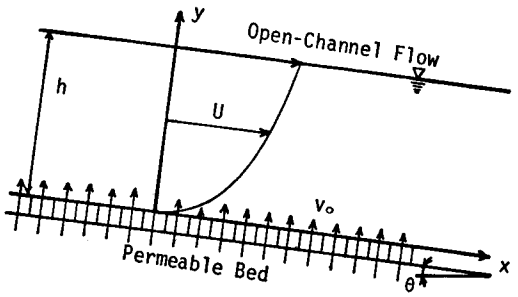

Fig. 1 Illustration of a permeable open-channel flow.

Near the wall ($\xi\ll 1$), (7) becomes

$$-\overline{uv}/U_*^2=1+v_0^+U^+-(dU^+/dy^+) \tag{8}$$

Since the mixing-length model may be valid in a *fully developed turbulent* shear flow,[7] the following relation can be obtained from (8).

$$\frac{dU^+}{dy^+}=\frac{2(v_0^+U^++1)}{1+\sqrt{1+4l^{+2}(v_0^+U^++1)}} \tag{9}$$

The mixing-length l^+ is given by the van Driest type[8], so that

$$l^+ \equiv \kappa_0 y^+ (1-\exp(-y^+/A^+)) \tag{10}$$

When $l^+ \ll 1$, (9) can be easily solved, as follows:

$$U^+ = \frac{1}{v_0^+}\{\exp(v_0^+ y^+) - 1\} \tag{11}$$

On the other hand, when $l^+ \gg 1$ or $l^+ \gg A^+$, (9) can be also solved, as follows:

$$\phi \equiv \frac{2}{v_0^+}(\sqrt{v_0^+ U^+ + 1} - 1) = \frac{1}{\kappa_0} \ln y^+ + D(v_0^+) \tag{12}$$

(12) is the bilogarithmic law, where κ_0 and D may be universal constants irrespective of transpiration, i. e. $\kappa_0 = 0.4$ and D=5.5. The damping factor A^+ is a function of v_0^+ since the viscous effect very near the wall may be remarkably varied by suction or injection. Consequently, by using A^+ which is determined so that the numerical solution of (9) may coincide with (12) at the edge of the wall region, i. e. $\delta^+ = 100$, we can obtain a universal law of the wall with transpiration throughout the wall region.

In order to examine the validity of the above consideration, the mean velocity distributions were measured in detail by a single-sensor hot-film anemometer (DISA type 55A83). Fig. 2 shows the experimental set-up in which the recirculating tilting flume is 15 m long, 50 cm wide and 30 cm deep. About 9 m downstream from the channel entrance, an apparatus of transpiration flow was set up, whose porous plate was 104 cm long, 49 cm wide and 1.5 cm thick. Through the preliminary experiments, it was recognized that a fully developed turbulent flow was obtained at the test section 84 cm downstream from the upstream edge of the porous plate.

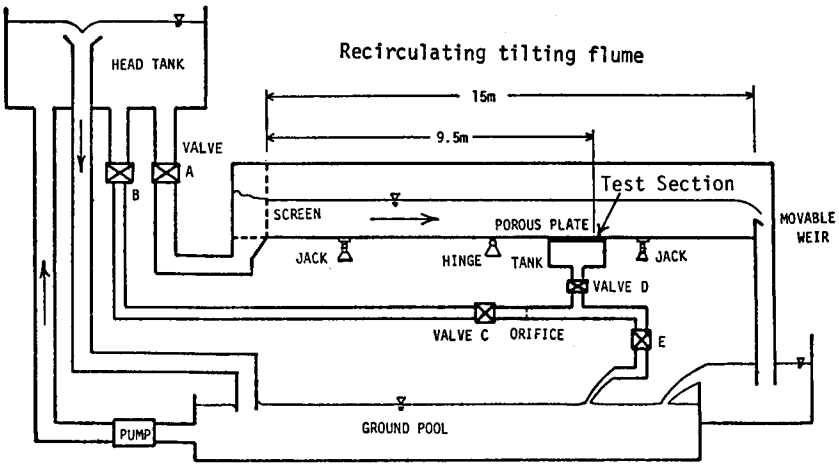

Fig. 2 Experimental set-up: a recirculating tilting flume and an apparatus of transpiration flow through the porous plate.

In the same manner as Kinny's(1967) method[9] in a boundary layer, the following relation can be obtained from (12).

$$\left(\frac{1-\sqrt{\Omega}-1.25\,\beta\ln\sqrt{\Omega}}{\sqrt{\Omega}}\right)\left(\frac{f_0}{2}\right)^{-1/2}-\frac{\beta}{4\sqrt{\Omega}}\left(\frac{f_0}{2}\right)^{-1}=2.5\ln\sqrt{\Omega}+\frac{\beta}{4\sqrt{\Omega}}\times\{(2.5\ln\sqrt{\Omega})^2+6.25\} \tag{13}$$

where, $\beta\equiv v_0/U_{*0}$, $f_0\equiv 2(U_{*0}/U_m)^2$

Since Nezu(1977)[10] has already established the method of evaluating U_{*0} from the Reynolds stress distribution $\tau/\rho=U_{*0}^2(1-\xi)$ in the case of a solid bed, the friction velocity $U_*=\sqrt{\Omega}\,U_{*0}$ with transpiration could be easily determined by (13) when β was given. (We call it the $\beta-\Omega$ method.)

Now, Fig. 3 shows an example of the dimensionless mean velocity distribution

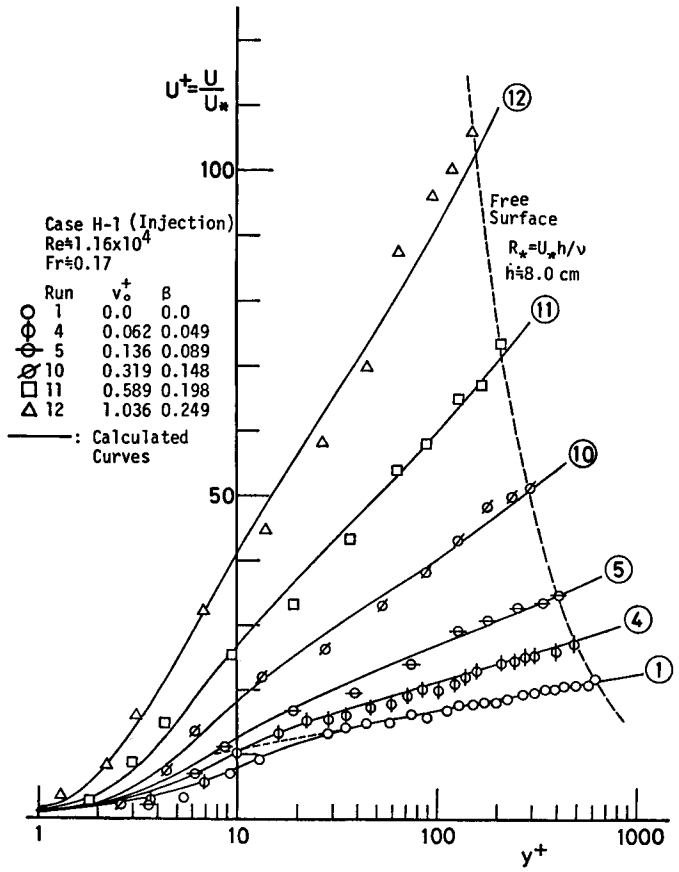

Fig. 3 Dimensionless mean velocity distribution $U^+=U/U_*$ with injection (the law of the wall).

$U^+ \equiv U/U_*$ with an injection obtained at the Reynolds number $Re = 1.16 \times 10^4$ and the Froude number $Fr = 0.17$. Run 1 is a case without transpiration, i. e. $v_0^+ = 0$, whose data coincided very well with the well-known law of the wall proposed by van Driest (1956)[8] or the Prandtl-Karman logarithmic law. The experimental values with injection showed a good agreement with the calculated curves of (9) throughout the whole region from the bed up to the free surface. That is to say, it was confirmed that the mixing-length model of (9) was valid even in the case of an open-channel flow with injection. Above all, even in the case of the large injection rate $v_0^+ \simeq 1$ where separation characteristics might appear, a good agreement was recognized.

On the other hand, Fig. 4 shows an example of the dimensionless mean velocity distribution U^+ with suction obtained at the same hydraulic condition as Fig. 3. It should be noticed that, although the agreement between the observed and the calculated values was still good at the moderate suction rate, the disagreement between them appeared in larger suction rates such as Run 14 and 15. From more detailed investigation,[11] we have concluded that when the suction rate $(-v_0^+)$ attains about 0.085 (in general, when the average gradient $-\langle \partial \tau^+/\partial y^+ \rangle$ of the shear stress in the wall region attains about 0.009), the open-channel flow cannot keep the turbulent state any longer and relaminarization characteristics appear.

Furthermore, we could obtain the following relation of the damping factor A^+ as a function of v_0^+:

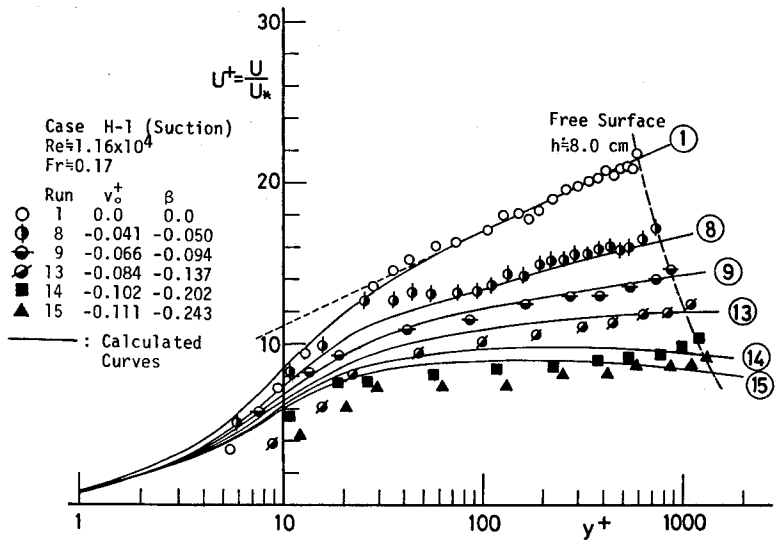

Fig. 4 Dimensionless mean velocity distribution U^+ with suction (the law of the wall).

$$A^+\begin{cases}=27/(1+4.1v_0^+) & \text{when suction is given.}\\ =27/(1+2.7v_0^+) & \text{when injection is given.}\end{cases} \tag{14}$$

When suction is given, the value of A^+ increases with $|v_0^+|$. Consequently, the viscous effect becomes stronger and thus relaminarization will appear.

3. Experimental equipment and data procedures in the present study

Two groups of experiments on two-dimensional fully developed turbulent flows in a permeable open-channel with suction or injection were conducted with the same experimental equipment as shown in Fig. 2. For reference, an experiment without transpiration (Run 1) was carried out under the conditions that the flow depth h was 8 cm, the Reynolds number Re was 1.3×10^4 and the Froude number Fr was 0.16, which were close to those of Figs. 3 and 4. One group was a suction group which consisted of four kinds of suction rate $\beta<0$. The other was an injection group which also consisted of four kinds of injection rate $\beta>0$. The friction velocity U_* in each run was evaluated by the $\beta-\Omega$ method since U_{*0} had been equal to 0.67 cm/sec. Table 1 shows the hydraulic parameters and the symbols in the following figures for each run.

The streamwise and normal components (u, v) of the instantaneous velocity were measured by using a set of constant-temperature anemometers with an X-type dual-sensor hot-film probe (DISA 55R63). The hot-film anemometers were calibrated by towing the probe over a fixed length (about 200cm) through still water, by making use of a movable carrier driven by a variable motor before and after each run. The output signals of the anemometers were recorded in analog form by using an FM tape recorder, and then were reproduced for conversion to digital form, in the same

Table 1 Hydraulic data for experiments with suction or injection and explanation of their symbols described in the following figures.

Symbol	Run	$\beta=v_0/U_{*0}$	U_*	$v_0^+=v_0/U_*$
■	13	−0.165	1.212	−0.091
⊖	9	−0.096	0.974	−0.066
▲	8	−0.052	0.830	−0.042
◑	7	−0.033	0.770	−0.029
●	1	0.0	0.670	0.0
◑	4	0.067	0.489	0.092
△	5	0.120	0.366	0.220
⊖	10	0.178	0.256	0.466
□	11	0.237	0.173	0.920

When $v_0=0$: $h=8.0$ cm, $U_m=14.1$ cm/s, $U_{*0}=0.67$ cm/s, $Re=1.3\times10^4$, $Fr=0.16$, $Tw=28.3$°C.

manner as described previously[3),4)]. In this study, the sample size N and the sampling frequency f were chosen as $N=10000$ and $f=100$ Hz at any measuring position. Consequently, the average-evaluation time $T=N/f$ became equal to 100 seconds. Some statistical analysis was carried out by means of conditional sampling with a large digital computer, the FACOM M-190, at the Data Processing Center, Kyoto University.

4. Experimental results and discussion

4.1 Distribution of Reynolds stress $-\overline{uv}$

The Reynolds stress $-\overline{uv}$ for each run was measured throughout the flow depth, and its distribution normalized by U_{*0} is shown in Fig. 5. The solid curves in this figure are theoretical ones calculated from (7) by using (4), (9) and (10), although the theoretical curve for Run 13 cannot be obtained here since the precondition of (4) and (9) is not satisfied for the stronger suction rate. This is due to the fact that relaminarization occurred in Run 13, since its value of $|v_0^+|$ is over the critical value $|v_0^+|\simeq 0.085$. Although there is some scattering in the measured data, the Reynolds stress $-\overline{uv}$ increases with an enlargement of the injection rate, while it decreases with an enlargement of the suction rate. It should be noticed that this transpiration effect appears more remarkably when closer to the wall. Hence, the effect of the transpiration upon the turbulent structure only near the wall will be discussed in the followings, since the bursting phenomenon or the turbulence production occurs most clearly in this region[2),3),4)]. Fortunately, the values of Reynolds stress measured near the wall have a fairly good agreement with the theoretical curves as seen in Fig. 5, and hence the accuracy of these data may be fairly good.

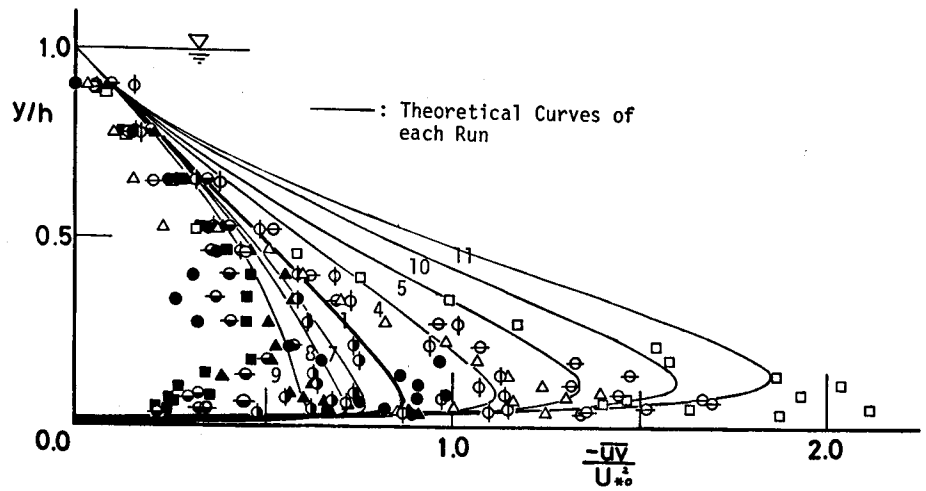

Fig. 5 Reynolds stress distribution $-\overline{uv}/U_{*0}^2$.

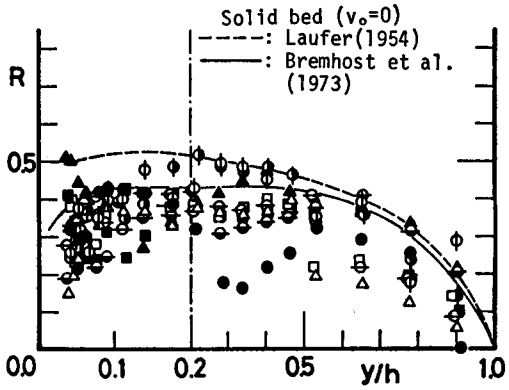

Fig. 6 Distribution of correlation coefficient $R=-\overline{uv}/u'v'$.

Next, Fig. 6 shows the distribution of the correlation coefficient $R\equiv-\overline{uv}/u'v'$ obtained at each run, where $u'\equiv(\overline{u^2})^{1/2}$ and $v'\equiv(\overline{v^2})^{1/2}$ are the turbulence intensities which will be described in the next section. Although the scattering of the measured data is comparatively large, the values of R near the wall are roughly equal to 0.2～0.4 irrespective of the transpiration, whose data coincide fairly well with those obtained over the solid bed.[6] This fact suggests that the turbulent structure has a strong characteristic of self-consistency of turbulence or similarity even when suction or injection exists, though the absolute values of u', v' and $-\overline{uv}$ are influenced remarkably by suction or injection.

4.2 Distribution of turbulence intensities

Fig. 7 shows the values of the streamwise turbulence intensity u'/U_{*0} against the dimensionless absolute coordinates $y_0^+\equiv yU_{*0}/\nu$ normalized by the inner parameters. The solid curve shown in this figure was obtained from the combined turbulent model, by which u'/U_{*0} without transpiration could be expressed fairly accurately in the whole region including the wall and equilibrium regions, and given by[6]

$$u'/U_{*0}=(1-\exp(-y^+/A))\cdot 2.3\exp(-y^+/R_*)+\exp(-y^+/A)\cdot By^+ \qquad (15)$$

where, $A=10$ and $B=0.3$.

In this study, the values of u'/U_{*0} without transpiration (Run 1) also agree very well with the curve of (15). When the injection is given, the turbulence intensity increases systematically, while it decreases in the wall region when the suction is given. Especially in Run 13 where relaminarization appeared, the turbulence intensity u' indicates a nearly uniform distribution against y_0^+. That is to say, when a strong suction rate is given, the maximum characteristic of u' may disappear in the buffer layer. This in-

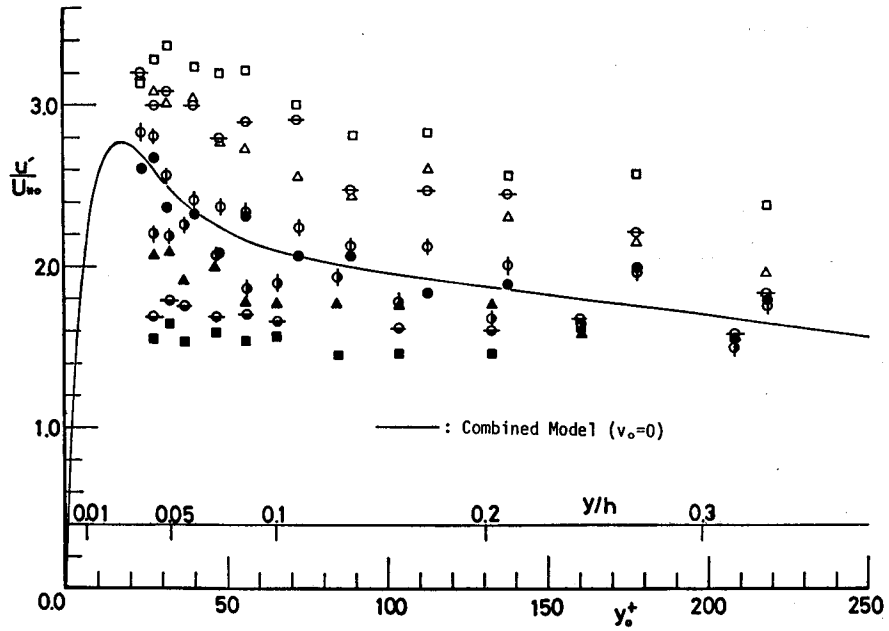

Fig. 7 Streamwise turbulence intensity u'/U_{*0}.

dicates that the bursting phenomenon or the turbulence production near the wall is probably suppressed by the strong suction.

Next, Fig. 8 shows the values of the normal turbulence intensity v'/U_{*0} against y_0^+. The solid curves in this figure were also obtained from the turbulent models over the solid bed proposed by the authors. The Ⓐ-curve was obtained from the renewal model[4] which was applicable in the wall region, and the Ⓑ-curve was obtained from the II-eddy model[6),10)] which was applicable in the equilibrium region. The observed

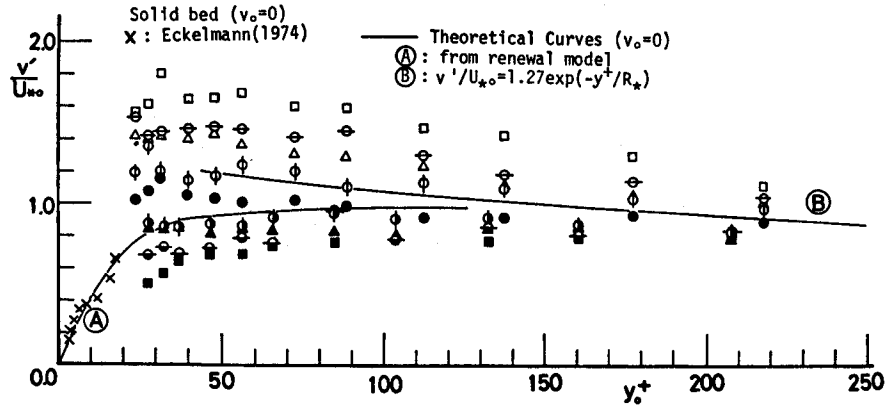

Fig. 8 Normal turbulence intensity v'/U_{*0}.

values of v'/U_{*0} without transpiration show a fairly good agreement with the Ⓐ and Ⓑ curves. v' close to the wall indicates an increase with an enlargement of the injection rate, while it indicates a little decrease with the suction rate. The same is true for u'

4.3 Probability density distributions of the velocity and Reynolds-stress fluctuations

Fig. 9 (a), (b) and (c) each show an example of the joint probability density distributions $p(\hat{u}, \hat{v})$ in the $\hat{u}$-$\hat{v}$ plane obtained without transpiration, with injection and with suction, respectively, where the velocity signals are normalized as $\hat{u} \equiv u/u'$ and $\hat{v} \equiv v/v'$. The isojoint probability density contours of $p(\hat{u}, \hat{v}) = 0.02, 0.05, 0.1, 0.15$ and 0.2 are described in these figures. Also, similar results were obtained for different measuring points and different rates of suction or injection. Although the observed contour curves have many ripples, they show roughly elliptic circles with respect to the principal axes, i. e. $\hat{v} = \pm \hat{u}$. Consequently, as a first approximation, $p(\hat{u}, \hat{v})$ can be described by the Gaussian distribution $G(\hat{u}, \hat{v})$ which is given by

$$G(\hat{u}, \hat{v}) \equiv \frac{1}{2\pi(1-R^2)^{1/2}} \exp\left\{-\frac{\hat{u}^2+2R\hat{u}\hat{v}+\hat{v}^2}{2(1-R^2)}\right\} \tag{16}$$

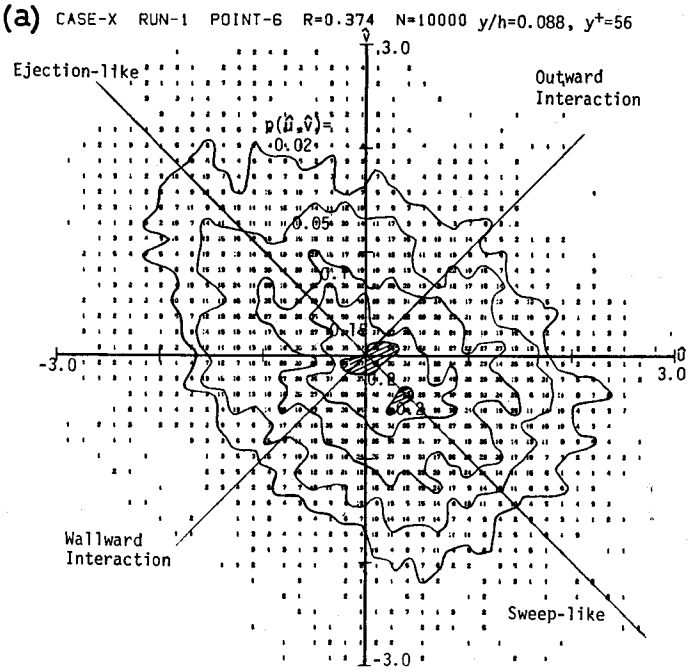

Fig. 9 (a) Isojoint probability density contour without transpiration (Run 1).

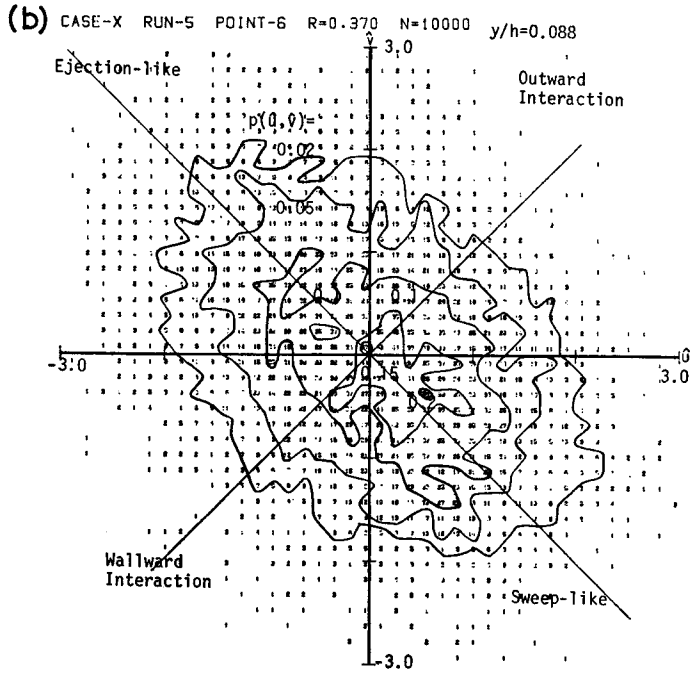

Fig. 9 (b) Isojoint probability density contour with injection (Run 5).

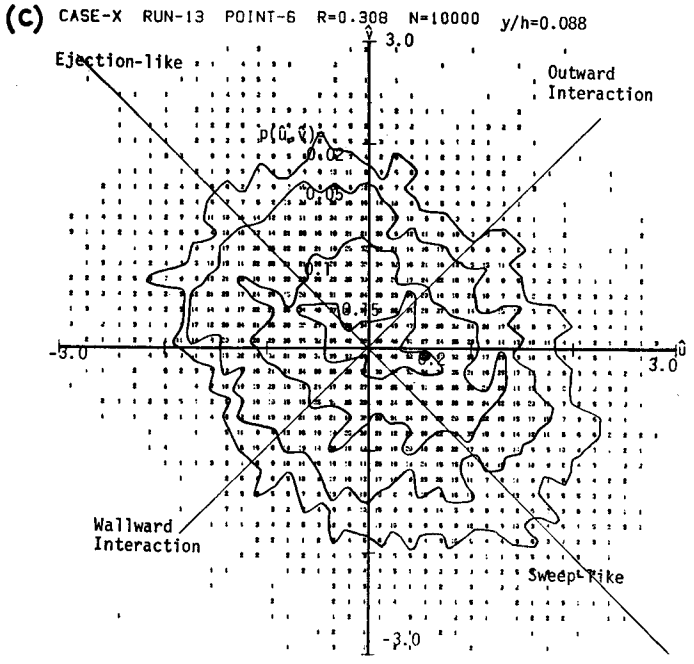

Fig. 9 (c) Isojoint probability density contour with strong suction (Run 13).

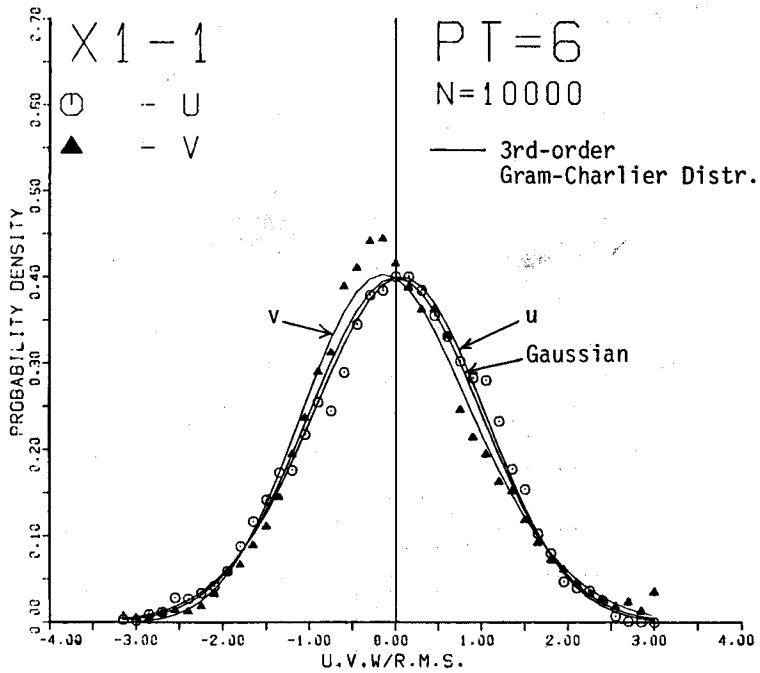

Fig. 10 Probability density distributions of u and v (Run 1).

Actually, the probability distributions $p(\hat{u})$ and $p(\hat{v})$ of $\hat{u}$ and $\hat{v}$, respectively, agree roughly with the Gaussian distribution, as shown in Fig. 10. However, it is recognized that these distributions indicate nearly symmetrical but small deviations to the positive and negative sides of the zero axis respectively; $p(\hat{u})$ having its maximum value on the positive side and its longer tail on the negative side, and vice versa for $p(\hat{v})$. This fact may be found more evidently in Fig. 9 since the maximum probability contour of $p(\hat{u}, \hat{v})$ appears near or in the fourth quadrant, i. e. $\hat{u}>0$ and $\hat{v}<0$ (Sweep-like event). These characteristics have been already verified in the case of a solid bed by the authors(1977)[3] and Wallace et al.(1977)[12]. Consequently, the skewness factors $S_u \equiv \overline{u^3}/u'^3$ and $S_v \equiv \overline{v^3}/v'^3$ became almost $S_u<0$ and $S_v>0$ irrespective of suction or injection, although the deviation from the Gaussian values, i. e. $S_u=0$ and $S_v=0$, was a little smaller except when very close to the wall in the case of suction only.

We (1977)[3] have pointed out in detail that the above-mentioned deviation from the Gaussian distribution should never be neglected essentially in order to make clear the bursting process, and that consequently at least the third-order Gram-Charlier distribution should be introduced, which is described by

$$p(\hat{u}, \hat{v}) = G(\hat{u}, \hat{v}) + \sum_{j+k=3} (-1)^{j+k} \frac{Q_{jk}}{j!k!} \frac{\partial^{j+k} G(\hat{u}, \hat{v})}{\partial \hat{u}^j \partial \hat{v}^k} \tag{17}$$

where Q_{jk} is the cumulant of (j, k)-order.

Then, denoting the probability distributions of Reynolds stress $w \equiv uv/\overline{uv}$ in each quadrant event by $p_1(w)$ (outward interaction, $u>0$ and $v>0$), $p_2(w)$ (ejection-like, $u<0$ and $v>0$), $p_3(w)$ (wallward interaction, $u<0$ and $v<0$) and $p_4(w)$ (sweep-like, $u>0$ and $v<0$), respectively, the following equations could be obtained from (17) by the authors[3].

$$\left.\begin{aligned} p_1(w) &= p_G(w) + \phi^+(w) \quad (w<0) \\ p_2(w) &= p_G(w) + \phi^-(w) \quad (w>0) \\ p_3(w) &= p_G(w) - \phi^+(w) \quad (w<0) \\ p_4(w) &= p_G(w) - \phi^-(w) \quad (w>0) \end{aligned}\right\} \tag{18}$$

where

$$p_G(w) = \frac{R}{2\pi} e^{Rt} \frac{K_0(|t|)}{(1-R^2)^{1/2}}, \tag{19}$$

$$\phi^+(w) = \frac{R}{2\pi} e^{Rt} K_{1/2}(|t|) \frac{|t|^{1/2}}{(1-R)^2} \left\{(1+R)\left(\frac{S^+}{3}+D^+\right)|t| - \left(\frac{2-R}{3}S^+ + D^+\right)\right\}, \tag{20}$$

$$\phi^-(w) = \frac{R}{2\pi} e^{Rt} K_{1/2}(t) \frac{t^{1/2}}{(1+R)^2} \left\{(1-R)\left(\frac{S^-}{3}+D^-\right)t - \left(\frac{2+R}{3}S^- + D^-\right)\right\} \tag{21}$$

and

$$S^{\pm} \equiv \frac{1}{2}(S_v \pm S_u) = \frac{1}{2}(Q_{03} \pm Q_{30}), \quad D^{\pm} \equiv \frac{1}{2}(D_v \pm D_u) = \frac{1}{2}(Q_{21} \pm Q_{12}). \tag{22}$$

K_ν is the νth-order modified Bessel function of the second kind. Also, D_u and D_v are the diffusion factors defined as $D_u = \overline{\hat{u}.\,\hat{v}^2}$ and $D_v = \overline{\hat{v}.\,\hat{u}^2}$.[3]

Thus, both the skewness and diffusion factors, which indicate a measure of the deviation from the Gaussian distribution, become the essential parameters in (20) and (21) in order to discuss the contribution of each event to the Reynolds stress, as will be described later.

Of course, the unconditional probability distribution $p_w(w)$ of Reynolds stress is given by

$$p_w(w) = p_1(w) + p_2(w) + p_3(w) + p_4(w). \tag{23}$$

Some examples of the observed values of $p_w(w)$ obtained from Fig. 9 are shown in Fig. 11, together with theoretical curves calculated from (23). The experimental values agree fairly well with the theoretical values. This good agreement between the two was also obtained in every other run. The skewness factor S_w and the flatness factor F_w of w were very large compared with S_u, S_v, F_u and F_v, that is, $S_w \simeq -2$ and $F_w \simeq 14$. Therefore, it is also verified that the Reynolds stress fluctuations have a strong intermittency, as pointed out previously[3),4].

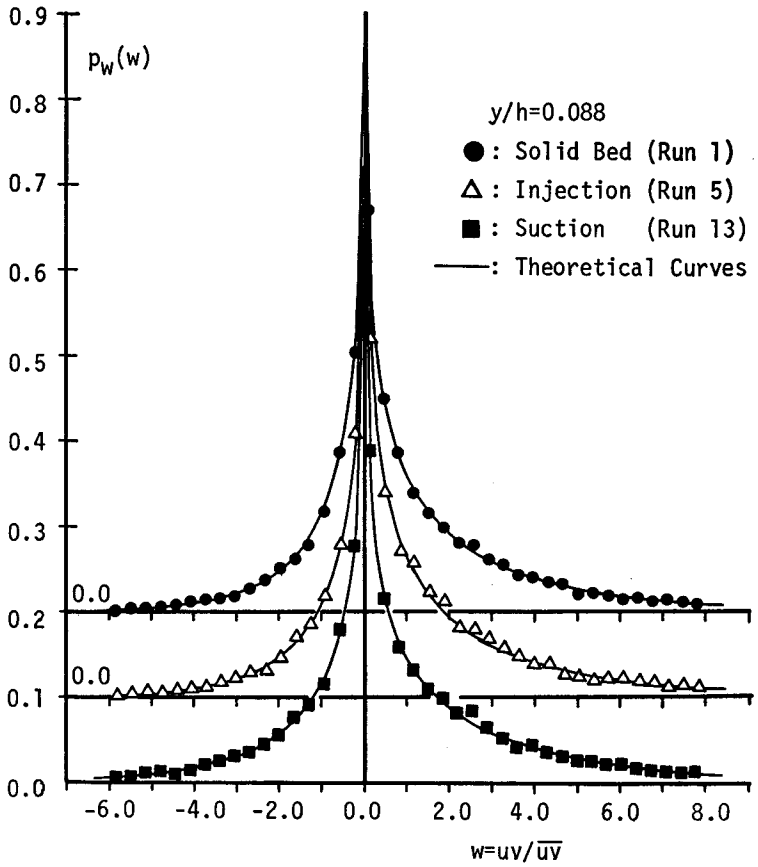

Fig. 11 Probability density distributions of the Reynolds-stress fluctuations.

4.4 Internal structure of the instantaneous Reynolds stress

In order to investigate the internal structure of the instantaneous Reynolds stress $\hat{w} \equiv -\hat{u}\hat{v} = Rw$ obtained from the $\hat{u}$-$\hat{v}$ plane in Fig. 9, the hole size H' is introduced here. Then, the fraction of time $T_i(H')$ occupied by each event with $\hat{w} \geq H'$ and the contributions $RS_i(H')$ of its event to the Reynolds stress are obtained by means of the same method of conditional sampling as that used by Lu & Willmarth (1973)[13]:

$$T_i(H') = \lim_{T\to\infty} \frac{1}{T} \int_0^T I_i(t, H')\, dt \qquad (i = 1, 2, 3, 4), \tag{24}$$

$$RS_i(H') = \frac{1}{\overline{uv}} \lim_{T\to\infty} \frac{1}{T} \int_0^T u(t) \cdot v(t) I_i(t, H')\, dt, \tag{25}$$

where

$$I_i(t, H') = \begin{cases} 1 & \text{for } |\hat{w}(t)| > H' \text{ and the point } (\hat{u}, \hat{v}) \text{ in the } i\text{th quadrant,} \\ 0 & \text{for } |\hat{w}(t)| \leq H'. \end{cases} \tag{26}$$

Some typical examples of the observed values obtained from (24) and (25) at the same position (i. e. $y/h=0.088$) in all experimental runs are plotted in Fig. 12, (a)-(i). The essential differences among the data of $T_i(H')$ and $RS_i(H')$ obtained at the other measuring positions are rarely recognized, although there is some scattering in the absolute values of these data. The theoretical curves described in Fig. 12 were calculated from the conditional probability distributions $p_i(w)$ $(i=1—4)$, as follows:

$$T_i(H)=\begin{cases}\int_H^{\infty} p_i(w)\,dw & (i=2,\ 4),\\ \int_{-\infty}^{-H} p_i(w)\,dw & (i=1,\ 3),\end{cases} \tag{27}$$

$$T_5(H)=\int_{-H}^{H} p_w(w)\,dw=1-\sum_{i=1}^{4} T_i(H) \quad \text{(the hole event)} \tag{28}$$

and

$$RS_i(H)=\begin{cases}\int_H^{\infty} wp_i(w)\,dw>0 & (i=2,\ 4),\\ \int_{-\infty}^{-H} wp_i(w)\,dw<0 & (i=1,\ 3),\end{cases} \tag{29}$$

$$RS_5(H)=\int_{-H}^{H} wp_w(w)\,dw=1-\sum_{i=1}^{4} RS_i(H) \quad \text{(the hole event)}. \tag{30}$$

where $H\equiv H'/R$.

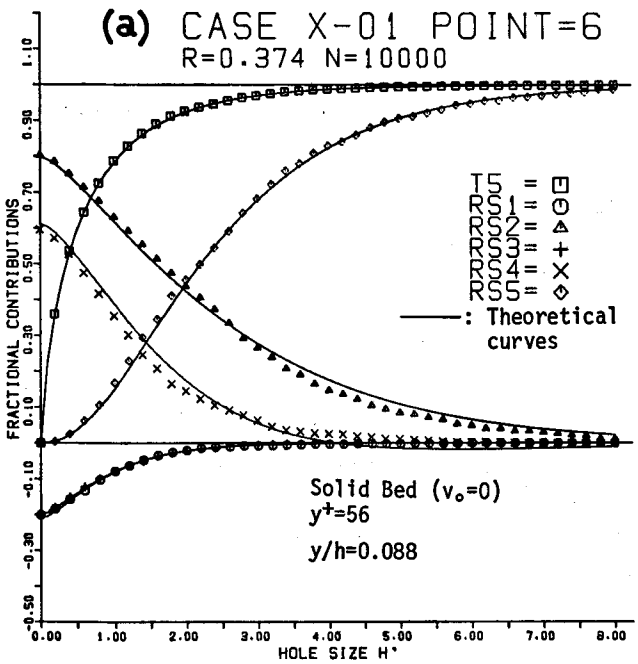

Fig. 12 (a) Internal structure of the instantaneous Reynolds-stress fluctuations. Without transpiration $v_0^+=0.0$.

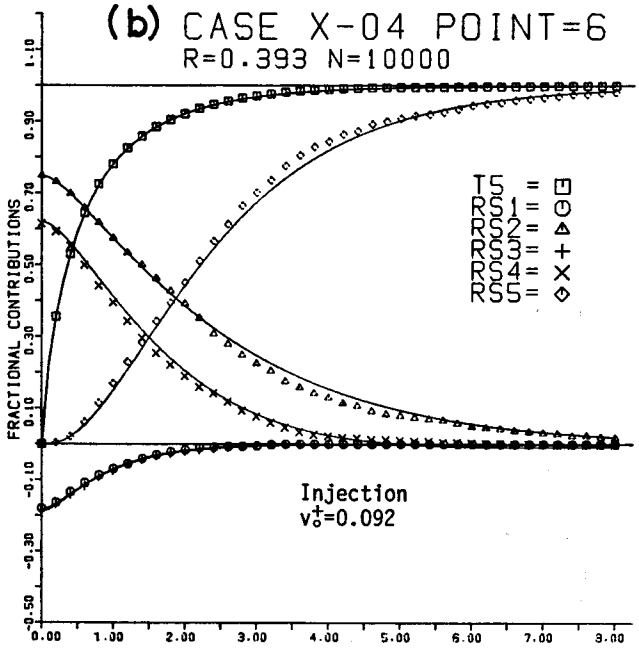

Fig. 12 (b) Injection v_0^+=0.092.

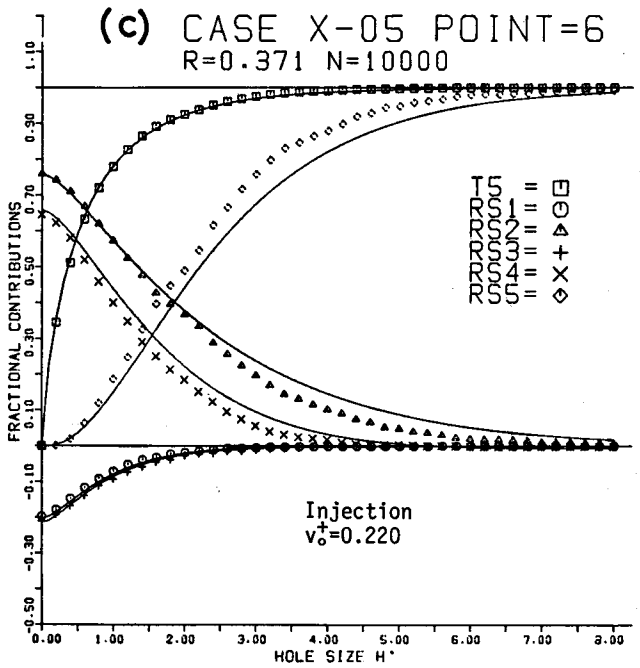

Fig. 12 (c) Injection v_0^+=0.220.

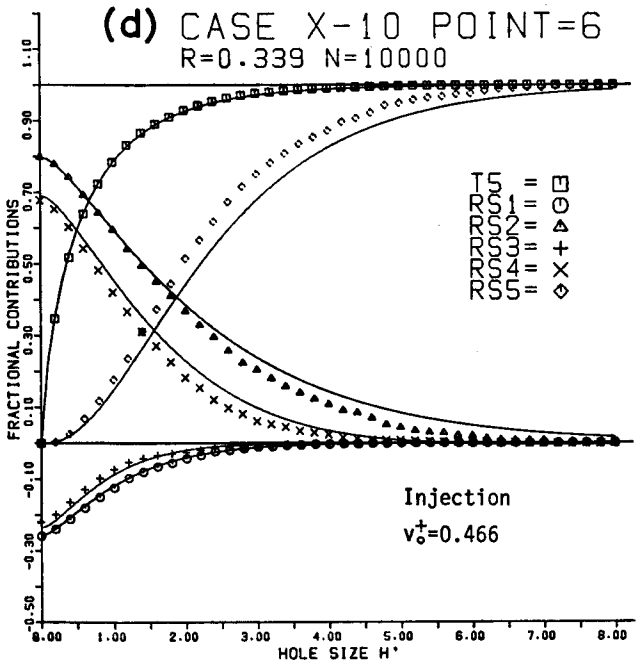

Fig. 12 (d) Injection v_0^+=0.466.

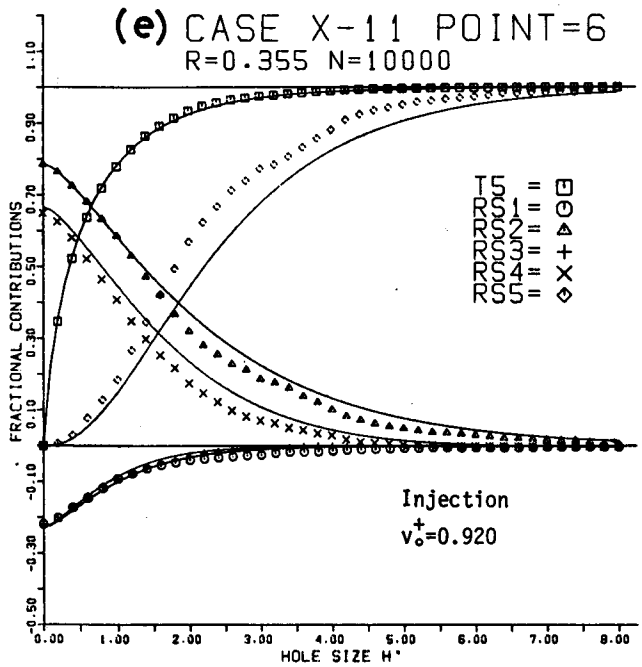

Fig. 12 (e) Injection v_0^+=0.920.

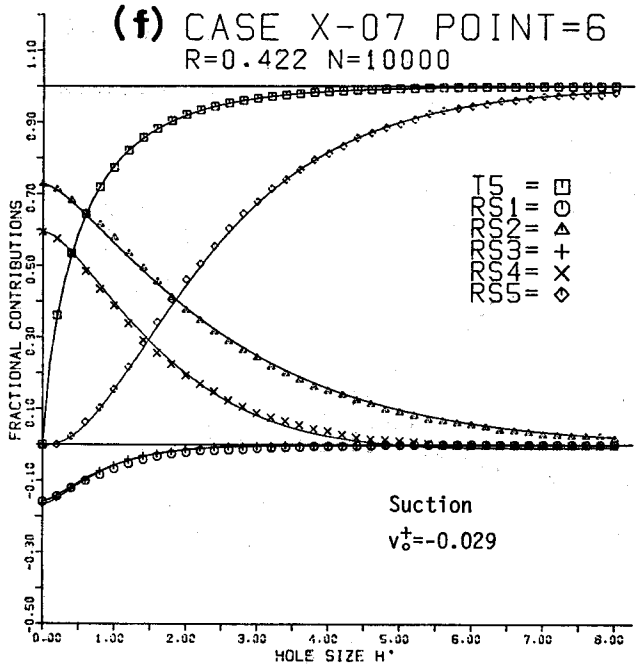

Fig. 12 (f) Suction $v_0^+=-0.029$.

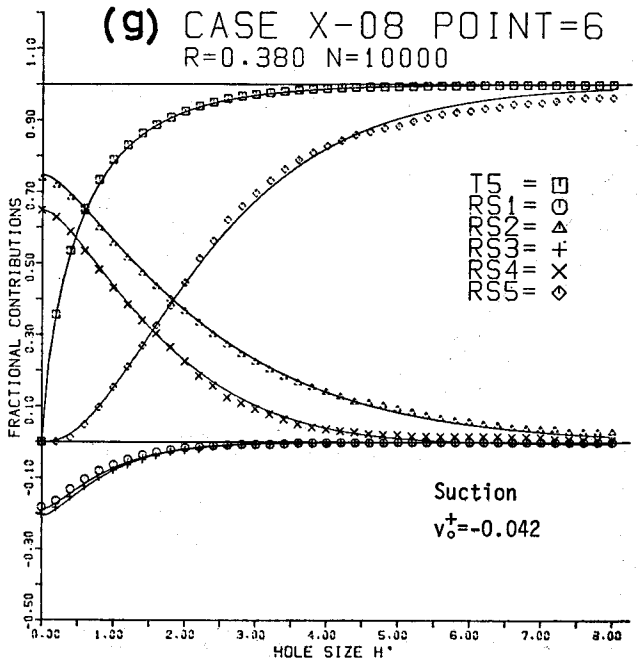

Fig. 12 (g) Suction $v_0^+=-0.042$.

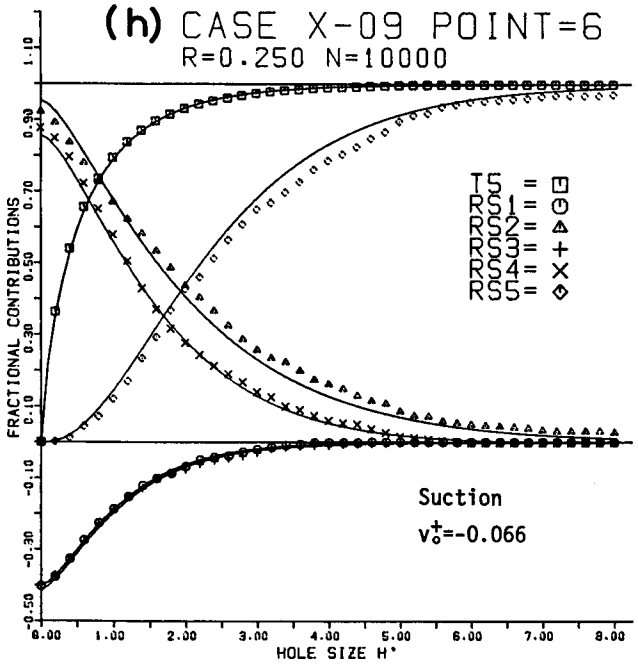

Fig. 12 (h) Suction v_0^+=—0.066.

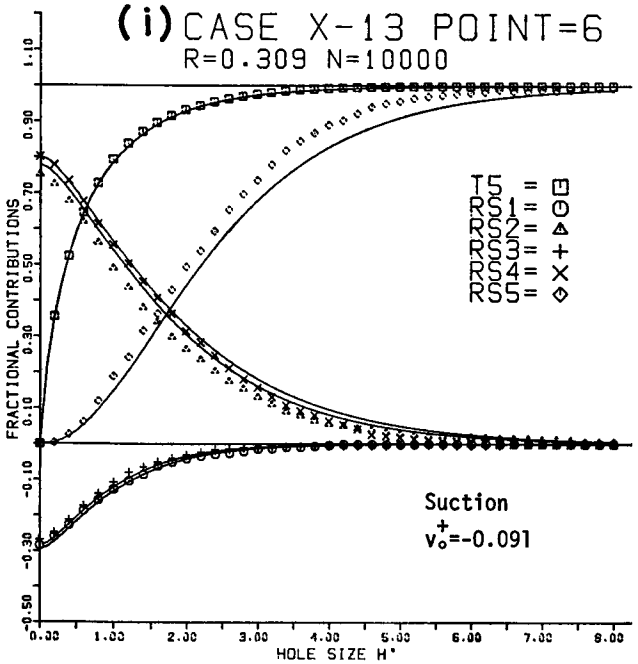

Fig. 12 (i) Suction v_0^+=—0.091.

The observed values of the fraction of time $T_5(H')$ occupied by the hole event ($|\hat{w}|<H'$) and the contributions $RS_i(H')$ ($i=1$—5) of each event agree fairly well with the theoretical curves, irrespective of the transpiration. This fact indicates that the third-order Gram-Charlier distribution can express fairly accurately the structure of the Reynolds stress in each bursting event even when the transpiration is given, as well as the case of the solid-wall turbulence[3]. As seen in Fig. 12 (a)-(e), the structure of the Reynolds stress for every injection run is almost the same as that for the case of non-transpiration, i. e. $v_0=0$. Also, its structure for the moderate suction rate is almost the same as that for the non-transpiration, although as the suction rate is larger, the magnitude of the sweeps(RS_4) may gradually approach that of the ejections (RS_2). Consequently, it is inferred that the internal structure of the turbulence itself may not be much influenced by suction or injection, but may have a strong self-similarity or self-consistency of turbulence. Since the detailed description of the characteristics of $RS_i(H')$ was given in our previous paper[3], its rewriting is omitted here. Fig. 12 indicates clearly that $RS_2>RS_4>|RS_1|\simeq|RS_3|$ for any hole size H'. This also confirms that the ejections RS_2 and the sweeps RS_4 may produce the turbulence or Reynolds stress, irrespective of suction or injection.

The ratio RS_4/RS_2 of contribution of the sweeps to the ejections with the hole size $H'=0$ is plotted for every run in Fig. 13, together with the results over a solid

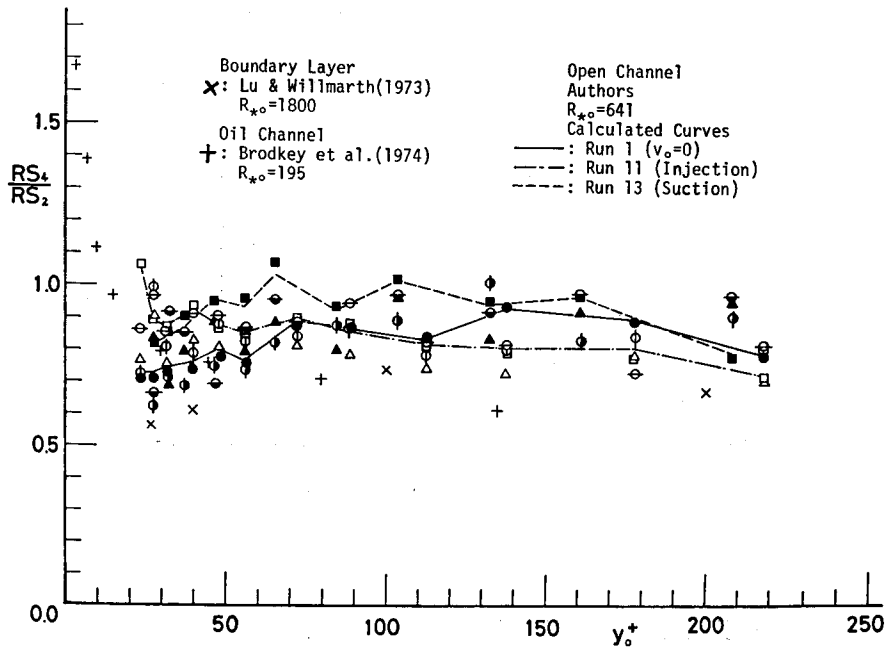

Fig. 13 The ratio RS_4/RS_2 of the sweeps to the ejections with $H'=0$ as a function of y_0^+.

bed obtained by Lu & Willmarth(1973)[13] and Brodkey et al.(1974)[14]. The theoretical values for $v_0=0$ (Run 1), the strong injection (Run 11) and the strong suction (Run 13), respectively, are also described by broken lines. It is generally noticed that the magnitude of the ejections is a little larger than that of the sweeps, i. e. $RS_2>RS_4$, independently of the transpiration.However, when the suction rate becomes as large as Run 13 where the turbulent state cannot be kept any longer, and thus relaminarization occurs as pointed out previously, the magnitude of the sweeps in the region of $y_0^+\gtrsim 50$ tends to become the same order as that of the ejections. This tendency of the relationship between the ejections and the sweeps has been also recognized in the case of a solid rough bed.[3] These may be caused by the fact that the turbulence characteristics with strong suction or the large roughness become uniform against the position of y_0^+, as seen in Figs. 7 and 8. Consequently, their skewness and diffusion factors as well as the turbulent diffusion rate decrease with an enlargement of suction or roughness, as was predicted by the authors[3].

On the other hand, as the injection rate become larger, the magnitude of the sweeps very close to the wall, i. e. $y_0^+\leq 50$, also tends to become the same order as that of the ejections. This is probably due to the characteristics of the viscous sublayer in which RS_4 becomes larger than RS_2, as seen in Brodkey et al's data, because the friction velocity U_* decreases with an increase of the injection rate. (See Chapter 2 or Table 1.) Consequently, the corresponding dimensionless position $y^+=U_*y/\nu$ also decreases with injection.

4.5 Mean period of the bursting process and its intensity

Lu & Willmarth(1973)[13], Brodkey et al. (1974)[14], Nakagawa & Nezu(1977[3], 1978[4]) and others have shown that the existence of a sequence of bursting events could be detectable even in the fluctuating velocity signals obtained by hot-wire or hot-film when a conditional sampling technique was reasonably used, as well as the various visual methods. Fig. 14 indicates an illustration of the fluctuating Reynolds-stress signals $-uv$ and its corresponding velocity signals u and v. As pointed out by Willmarth(1975)[2], it is the most important but difficult matter how to determine a reasonable criterion for discriminating the ejections or the sweeps which can be observed visually, from the ejection-like ($u<0$, $v>0$) or the sweep-like ($u>0$, $v<0$) events in the Reynolds-stress signals, respectively. That is to say, it is necessary to reasonably determine the threshold level (the hole size) H', whereby the ejections or the sweeps are assumed to occur when the Reynolds-stress signals $\hat{w}(t)=-u(t)v(t)/u'v'$ reach or exceed level H', as shown in Fig. 14. For example, Lu & Willmarth(1973)[13] decided that the threshold level H_e' of the ejections was $H_e'=4.0$—4.5 at which the contributions of the sweeps to Reynolds stress almost disappeared. They also thought

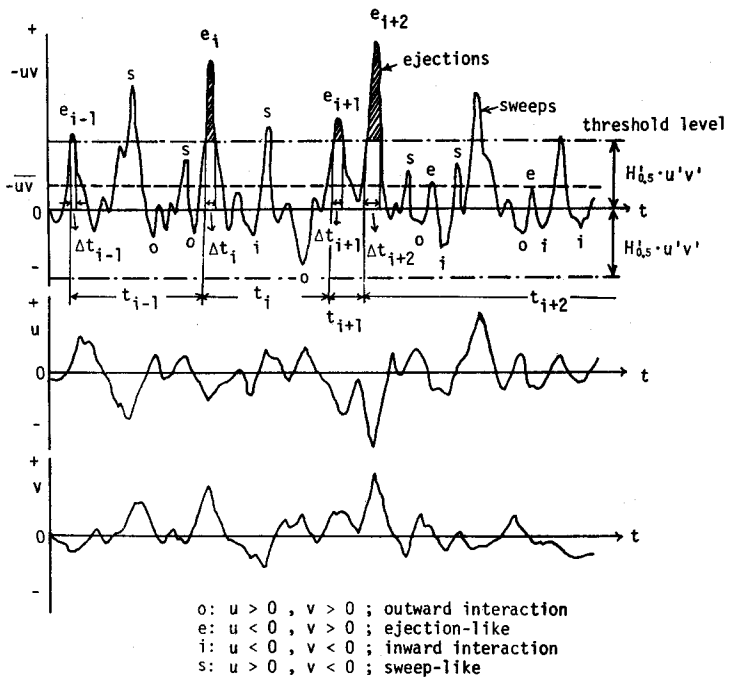

Fig. 14 Illustration of the fluctuating Reynolds-stress signals and its corresponding velocity signals u and v.

that the threshold level H_s' of the sweeps was $H_s'=2.25—2.75$ at which the contributions of the interactions almost disappeared, as seen in Fig. 12. However, the variation range of the mean ejection period $\overline{T}_e$ or the mean sweep period $\overline{T}_s$ evaluated from the above threshold levels of Lu & Willmarth, was too large to know the effects of hydraulic parameters such as Re, Fr and the wall roughness upon the bursting period systematically.[4] So, the authors (1978)[4] have proposed a new evaluation method for the bursting period, on the basis of the phenomenological consideration that the number of the occurrences of interaction-like motions should be removed from those of the ejection-like or the sweep-like events in the sorted Reynolds-stress fluctuating signals. Then, by using this interaction-cancellation method, we could evaluate uniquely the values of $\overline{T}_e$ or $\overline{T}_s$. Our evaluation method as well as Lu & Willmarth's method is based on the internal structure of Reynolds stress, described in Fig. 12. Consequently, the effect of the transpiration upon the bursting period $\overline{T}_e$ or $\overline{T}_s$ evaluated by the above method will be not quite recognized, because the structures of Reynolds stress are almost the same independently of the transpiration, as mentioned previously.

Hence, we tentatively propose a similar but more flexible evaluation method as compared with our previous method. That is, the threshold level $H'_{0.5}$ is here defined,

as follows:

$$RS_2(H'_{0.5}) \equiv 0.5RS_2(H'=0) \tag{31}$$

By counting the number N of the occurrences of ejections in which the Reynolds-stress signals $w_2(t) \equiv -uv$ reach or exceed $H'_{0.5} \cdot u'v'$ as shown by the hatch in Fig. 14, the mean ejection period $\overline{T}_e$ can be given by

$$\overline{T}_e = \frac{1}{N}\sum_{i=1}^{N} t_i = \frac{T}{N} \tag{32}$$

The results of $\overline{T}_e$ obtained from (31) and (32) are shown in Fig. 15, normalized by the outer parameters (U_{max} and h). As was expected, even when suction or injection is given, the ejection period $\overline{T}_e U_{max}/h$ becomes nearly equal to 2 independently of the position y_0^+. Also, the sweep period $\overline{T}_s U_{max}/h$ evaluated by the same manner as (31) showed similar results. These results coincide fairly well with the data over a solid bed evaluated by the interaction-cancellation method by the authors,[4] since the interaction events almost disappear at the threshold level $H'_{0.5} \simeq 2$, as seen in Fig. 12. Obviously, the values of $\overline{T}_e$ by Lu & Willmarth are a little larger than our data because their threshold level is larger than our level.

In order to investigate the effects of transpiration upon the bursting period, an '*absolute*' criterion for discriminating the occurrences of ejections from the ejection-like signals($u<0$, $v>0$) should be introduced. So, it is assumed that the '*absolute*' ejections occur when the Reynolds-stress signals $w_2(t)$ in the ejection-like event reach or exceed the '*absolute*' level $H'_{0.5} \cdot u'_0 \cdot v'_0$, where u'_0 and v'_0 are the corresponding turbulence intensities in the case of non-transpiration. That is to say, since $u'_0/U_{*0} \simeq 2$, $v'_0/U_{*0} \simeq 1$(see Figs. 7 and 8) and $H'_{0.5} \simeq 2$, the '*absolute*' ejections occur when $w_2(t) \geq H'_{0.5}u'_0v'_0 \simeq 4U^2_{*0}$, independently of the transpiration rate.

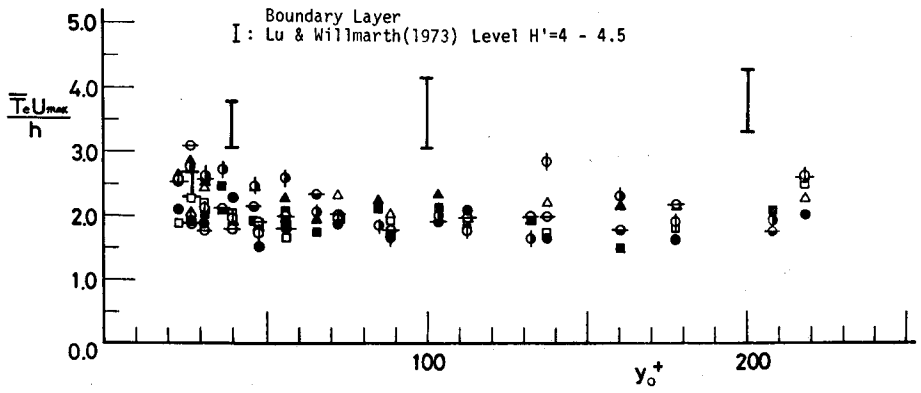

Fig. 15 Mean period $\overline{T}_e U_{max}/h$ of ejections as a function of y_0^+.

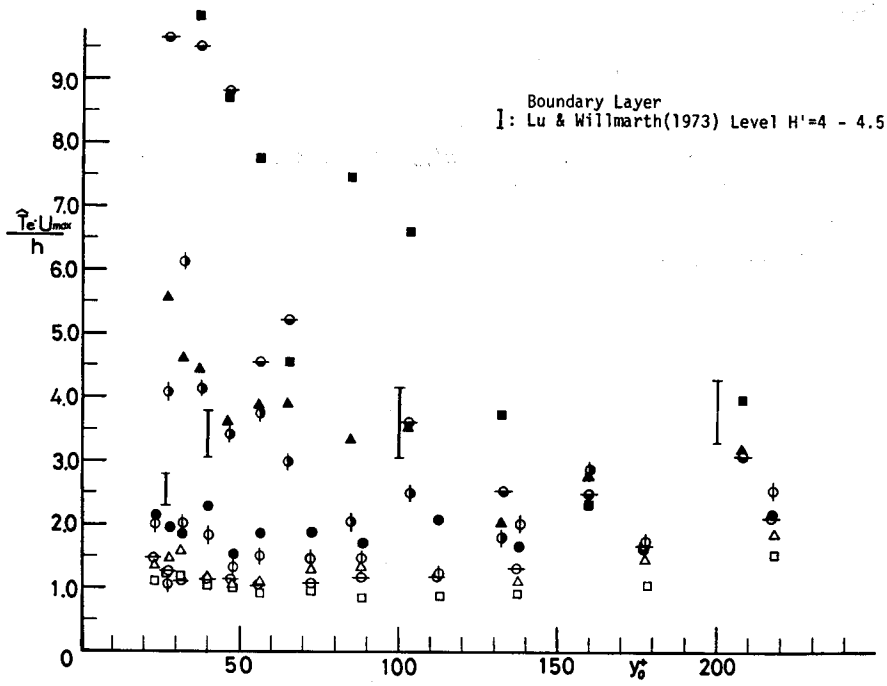

Fig 16 Mean period $\hat{T}_e U_{max}/h$ of 'absolute' ejections as a function of y_0^+.

Fig. 16 shows the mean period $\hat{T}_e$ of the absolute ejections obtained at the above level. The ejection period $\hat{T}_e$ decreases a little with an enlargement of the injection rate, while it increases remarkably, especially near the wall, with an enlargement of the suction rate. The same results are also obtained for the *'absolute'* sweeps. These results indicate that the occurrences of the bursting process are promoted a little by injection, while they are suppressed remarkably by strong suction.

Now, the intensity $-\langle uv\rangle_e$ of the absolute ejections is defined as an average of each ejection motion whose intensity is also averaged over the interval of its occurrence duration Δt_i (see Fig. 14). That is,

$$-\langle uv\rangle_e \equiv \frac{1}{N}\sum_{i=1}^{N}\left\{\frac{1}{\Delta t_i}\int_0^{\Delta t_i} w_2(t)\,dt\right\} \tag{34}$$

Also, the mean occurrence duration ΔT_e of the ejections is given by

$$\Delta T_e = \frac{1}{N}\sum_{i=1}^{N}\Delta t_i \tag{35}$$

The experimental values of $-\langle uv\rangle_e/U_{*0}^2$ and $\Delta T_e U_{max}/h$ are shown in Figs. 17 and 18, respectively. In the region of $y_0^+ \geq 50$, the intensity of ejections becomes a little stronger with injection, while for suction it becomes a little weaker and it may ap-

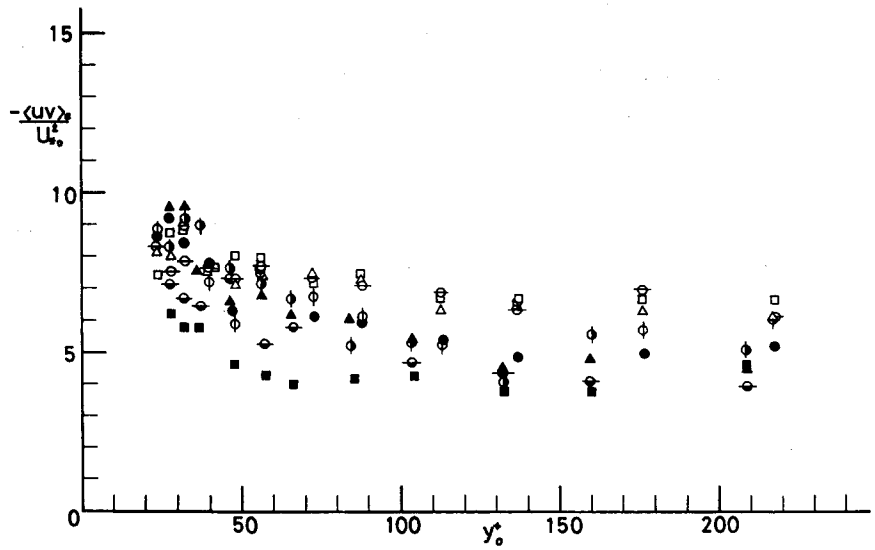

Fig. 17 Intensity $-\langle uv\rangle_*/U_{*0}^2$ of 'absolute' ejections.

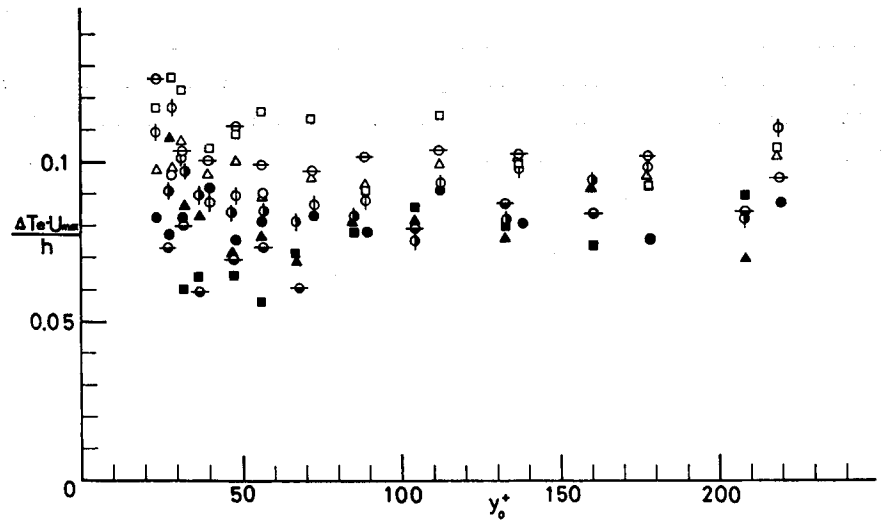

Fig. 18 Mean occurrence duration $\Delta T_* U_{max}/h$ of 'absolute' ejections.

proach the threshold value of about $4U_{*0}^2$ in the case of relaminarization such as Run 13. However, the intensity of the ejections in the region of $y_0^+ \leq 50$ may hardly be influenced by the transpiration. On the other hand, the effect of the transpiration upon the duration of ejections may appear more clearly closer to the wall.

It should be noticed that the ejection period $\overline{T}_*$ or $\hat{T}_*$ and its duration time ΔT_*

may scale with the outer parameter rather than the inner parameter even when suction or injection is given, since their expression by the inner parameter, e. g. $\bar{T}_s U_*^2/\nu$, is varied very much by the transpiration (cf. Table 1). This suggests that an initial condition of occurrence of the bursting process may be determined by the flow characteristics in the equilibrium region (outer layer) rather than in the wall region (inner layer). Consequently, the effect of the transpiration upon the bursting phenomenon, as well as the effect of the wall roughness upon it,[4] may be comparatively small, and thus the structure of their turbulence itself may become self-similar. Also, since the turbulence production is nearly in proportion to $-<uv>_s \Delta T_s/\dot{T}_s$, the promotion of turbulence by injection may be caused by the increase of three parameters of $-<uv>_s$, ΔT_s and $1/\dot{T}_s$, while the suppression of turbulence by strong suction may be caused mainly by the decrease of $1/\dot{T}_s$, although detailed investigations will be further needed.

5. Conclusions

In the present study, we have investigated experimentally the structure of the instantaneous Reynolds stress over a permeable bed with suction or injection in open-channel flow by means of conditionally analyzing its fluctuating signals obtained from X-type hot-films, in order to examine the effect of suction or injection on the turbulence production mechanism or the bursting phenomenon. The absolute magnitudes of the turbulence intensities and the Reynolds stress near the wall increased with an increase of injection, while they decreased with an increase of suction. However, the fraction of time occupied by each bursting event and the contributions of its event to the Reynolds stress against any hole size were almost the same, irrespective of suction or injection. So, it has been generally recognized that the magnitude of the ejections was a little larger than that of the sweeps independently of the transpiration, although the magnitudes of the two became of the same order at the extremely strong suction where relaminarization occured. The promotion of turbulence by injection or its suppression by suction may be caused by similar variations of three parameters of the bursting intensity, the bursting period and the bursting duration time. To sum up, the internal structure of the turbulence or the bursting mechanism may not be essentially influenced by suction or injection, as long as the flow is still turbulent.

References

1) Hinze, J. O.: *Turbulence* (2nd ed.), McGraw-Hill, pp. 586-770 (1975).
2) Willmarth, W. W.: Structure of turbulence in boundary layers, Adv. Appl. Mech., vol. **15**, pp. 159-254 (1975).
3) Nakagawa, H. and Nezu, I.: Prediction of the contributions to the Reynolds stress from the bursting events in open-channel flows, J. Fluid Mech., vol. 80, pp. 99-128 (1977).

4) Nakagawa, H. and Nezu, I.: Bursting phenomenon near the wall in open-channel flows and its simple mathematical model, THIS MEMOIRS, Fac. Eng., Kyoto University, vol. **40**, pp. 213-240 (1978).
5) Andersen, P. S., Kays, W. M. and Moffat, R. J.: Experimental results for the transpired turbulent boundary layer in an adverse pressure gradient, J. Fluid Mech., vol. **69**, pp. 353-375 (1975).
6) Nezu, I.: *Turbulent structure in open-channel flows*, Dr. Eng. Thesis presented in Kyoto University (1977).
7) Bradshaw, P.: Mixing-length velocity profile in boundary layers with transpiration, AIAA J., vol. **5**, pp. 1674-1675 (1967).
8) van Driest, E. R.: On turbulent flow near a wall, J. Aero. Sci., vol. **23**, pp. 1007-1011 (1956).
9) Kinney, R. B.: Skin-friction drag of a constant-property turbulent boundary layer with uniform injection, AIAA J., vol. **5**, pp. 624-630 (1967).
10) Nezu, I: Turbulence intensities in open channel flows, Proc. Japan Soc. Civil. Engrs, No. **261**, pp. 67-76 (1977) (in Japanese).
11) Nakagawa, H. and Nezu, I.: Turbulent structure in permeable open-channel flows with transpiration, Proc. Japan Soc. Civil Engrs, No. **285**, pp. 45-56 (1979) (in Japanese).
12) Wallace, J. M. and Brodkey, R. S.: Reynolds stress and joint probability density distributions in the u-v plane of a turbulent channel flow, Phys. of Fluids, vol. **20**, pp 351-355 (1977).
13) Lu, S. S. and Willmarth, W. W.: Measurements of the structure of the Reynolds stress in a turbulent boundary layer, J. Fluid Mech., vol. **60**, pp. 481-511 (1973).
14) Brodkey, R. S., Wallace, J. M. and Eckelmann, H.: Some properties of truncated turbulence signals in bounded shear flows, J. Fluid Mech., vol. **63**, pp. 209-224 (1974).